Title
The glucocorticoid-Angptl4-ceramide axis induces insulin resistance through PP2A and PKCζ

Journal
Science Signaling, 10(489)

ISSN
1945-0877

Authors
Chen, Tzu-Chieh
Benjamin, Daniel I
Kuo, Taiyi
et al.

Publication Date
2017-07-25

DOI
10.1126/scisignal.aai7905

Peer reviewed

METABOLISM

The glucocorticoid-Angptl4-ceramide axis induces insulin resistance through PP2A and PKCζ

Tzu-Chieh Chen,[1,2] Daniel I. Benjamin,[1,2] Taiyi Kuo,[2,3] Rebecca A. Lee,[2,3] Mei-Lan Li,[2] Darryl J. Mar,[2] Damian E. Costello,[2,3] Daniel K. Nomura,[1,2,3,4] Jen-Chywan Wang[1,2,3]*

Chronic glucocorticoid exposure is associated with the development of insulin resistance. We showed that glucocorticoid-induced insulin resistance was attenuated upon ablation of *Angptl4*, a glucocorticoid target gene encoding the secreted protein angiopoietin-like 4, which mediates glucocorticoid-induced lipolysis in white adipose tissue. Through metabolomic profiling, we revealed that glucocorticoid treatment increased hepatic ceramide concentrations by inducing enzymes in the ceramide synthetic pathway in an Angptl4-dependent manner. Angptl4 was also required for glucocorticoids to stimulate the activities of the downstream effectors of ceramide, protein phosphatase 2A (PP2A) and protein kinase Cζ (PKCζ). We further showed that knockdown of PP2A or inhibition of PKCζ or ceramide synthesis prevented glucocorticoid-induced glucose intolerance in wild-type mice. Moreover, the inhibition of PKCζ or ceramide synthesis did not further improve glucose tolerance in *Angptl4*$^{-/-}$ mice, suggesting that these molecules were major downstream effectors of Angptl4. Overall, our study demonstrates the key role of Angptl4 in glucocorticoid-augmented hepatic ceramide production that induces whole-body insulin resistance.

INTRODUCTION

Insulin resistance is a major risk factor for type 2 diabetes and cardiovascular diseases. Chronic and/or excess glucocorticoid exposure has been associated with the development of insulin resistance (*1*–*3*). Glucocorticoids reduce insulin-stimulated glucose utilization in skeletal muscle and white adipose tissue (WAT). Glucocorticoid exposure also suppresses insulin responsiveness in the liver and potentiates gluconeogenesis, which is inhibited by insulin. Several mechanisms have been proposed to explain glucocorticoid-induced insulin resistance. One mechanism is that glucocorticoids directly inhibit insulin signaling and insulin-stimulated glucose uptake in myotubes and adipocytes (*4*–*7*). A second mechanism is that osteocalcin secreted from bone promotes insulin secretion and sensitivity (*8*). A third mechanism is that lipolysis in WAT induced by glucocorticoids leads to insulin resistance. Several lines of evidence support this mechanism. Administration of acipimox, an inhibitor of WAT lipolysis, reduces glucocorticoid-induced insulin resistance in humans (*9*). Similarly, injecting nicotinic acid into male Sprague-Dawley rats to decrease WAT lipolysis corrects the antagonistic effects of glucocorticoids on insulin actions (*10*). A final mechanism is that glucocorticoid treatment increases hepatic ceramide concentrations. One line of evidence supporting this mechanism is that inhibition of ceramide synthesis by the small-molecule inhibitor myriocin compromises glucocorticoid-induced insulin resistance (*11*). Also, the ability of glucocorticoids to cause insulin resistance is reduced in mice lacking Des2, an enzyme in the ceramide biosynthesis pathway (*11*).

The biological responses of glucocorticoids are mainly mediated by the glucocorticoid receptor, which directly regulates its primary target genes. Therefore, to understand the molecular mechanism of glucocorticoid-induced insulin resistance, the first step is to identify glucocorticoid receptor primary target genes that participate in this glucocorticoid-regulated process. We have previously identified *Angptl4* (which encodes angiopoietin-like 4) as a glucocorticoid receptor primary target gene in hepatocytes and adipocytes (*12*, *13*). The *Angptl4* gene encodes a secreted protein that promotes lipolysis in adipocytes (*14*) and inhibits extracellular lipoprotein lipase (LPL) (*15*, *16*). *Angptl4*$^{-/-}$ mice display impaired glucocorticoid-induced WAT lipolysis (*14*) and are therefore excellent models for assessing the role of WAT lipolysis in glucocorticoid-modulated metabolite changes in peripheral tissues that cause insulin resistance.

Here, we analyzed the effects of glucocorticoids on glucose homeostasis and insulin actions in *Angptl4*$^{-/-}$ mice. We also performed metabolomics in the liver and skeletal muscle of *Angptl4*$^{+/+}$ (which will be called wild-type mice) and *Angptl4*$^{-/-}$ mice treated with or without glucocorticoids. Our goal was to establish *Angptl4* as a glucocorticoid receptor primary target gene that potentially links glucocorticoid-promoted WAT lipolysis to the changes of insulin resistance–inducing metabolites in the liver and/or skeletal muscle and to elucidate the mechanism governing this process.

RESULTS

Glucocorticoid-induced insulin resistance was improved in *Angptl4*$^{-/-}$ mice

Wild-type and *Angptl4*$^{-/-}$ mice were treated with or without dexamethasone (a synthetic glucocorticoid) for 7 days. Intraperitoneal glucose tolerance tests (IPGTTs) showed that in the absence of dexamethasone treatment, there was no significant difference in basal glucose tolerance between wild-type and *Angptl4*$^{-/-}$ mice (Fig. 1, A and B). Dexamethasone treatment induced glucose intolerance in wild-type mice, as expected, but not in *Angptl4*$^{-/-}$ mice (Fig. 1, A and B). Furthermore, fasting plasma insulin concentrations were markedly higher in dexamethasone-treated wild-type mice than those in untreated wild-type and *Angptl4*$^{-/-}$ mice or in dexamethasone-treated *Angptl4*$^{-/-}$ mice (Fig. 1C, 0 min). These results confirmed that dexamethasone treatment in mice caused insulin resistance resulting in hyperinsulinemia. Moreover, the decreased glucose tolerance in dexamethasone-treated wild-type mice despite the presence of hyperinsulinemia suggested that pancreatic islet β cells could not compensate for insulin resistance. In untreated wild-type

[1]Metabolic Biology Graduate Program, University of California, Berkeley, Berkeley, CA 94720–3104, USA. [2]Department of Nutritional Sciences and Toxicology, University of California, Berkeley, Berkeley, CA 94720–3104, USA. [3]Endocrinology Graduate Program, University of California, Berkeley, Berkeley, CA 94720–3104, USA. [4]Departments of Chemistry and Molecular and Cell Biology, University of California, Berkeley, Berkeley, CA 94720–3104, USA.
*Corresponding author. Email: walwang@berkeley.edu

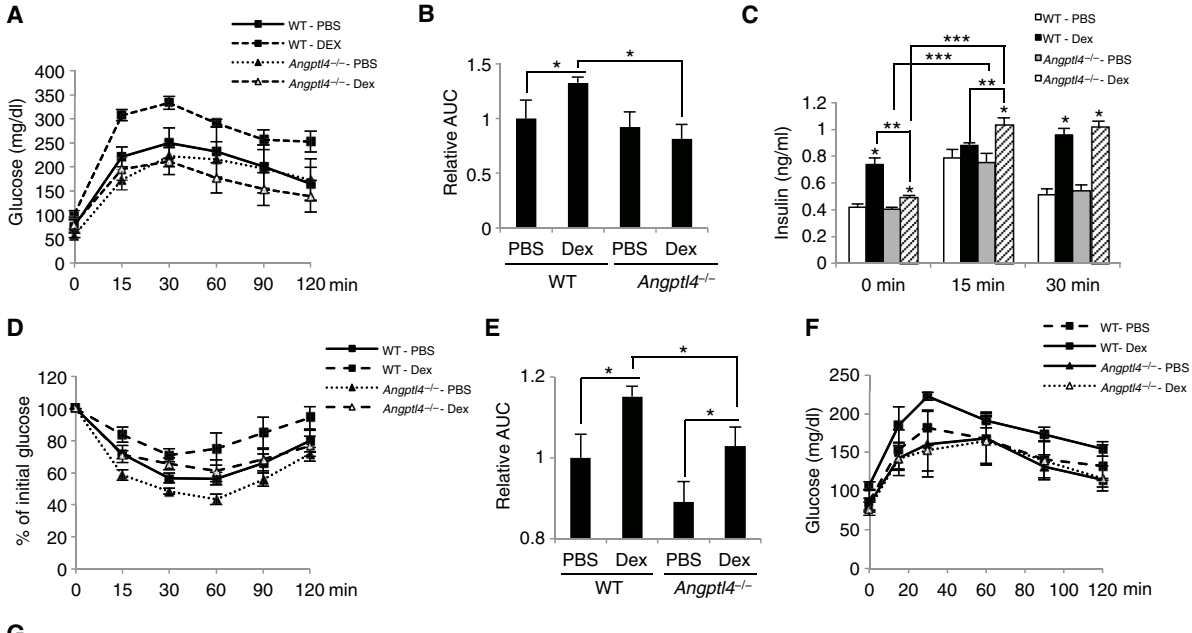

Fig. 1. Dexamethasone-induced glucose, insulin, and pyruvate intolerance were improved in *Angptl4*$^{-/-}$ mice. Wild-type (WT) and *Angptl4*$^{-/-}$ mice were treated with phosphate-buffered saline (PBS) or dexamethasone (Dex). (**A**) GTT was performed after 16 hours of fasting. (**B**) Relative area under curve (AUC) for GTT results (relative to PBS-treated WT mice) is shown. Error bars represent SEM. $n = 5$ to 7 mice per group. *$P < 0.05$. (**C**) Plasma insulin concentrations were measured before glucose injection (0 time point), and 15 and 30 min after glucose injection. Error bars represent SEM. $n = 5$ to 7 mice per group. * indicates significant ($P < 0.05$) effect of dexamethasone (compared to PBS) at the given time point, ** indicates significant difference ($P < 0.05$) between WT dexamethasone and *Angptl4*$^{-/-}$ dexamethasone at the given time point, and *** indicates significant ($P < 0.05$) difference between time points. (**D**) ITT was performed, and results are displayed as percentage of initial plasma glucose concentrations at different time points. (**E**) Relative AUC for ITT results (relative to PBS-treated WT mice) is shown. Error bars represent SEM. $n = 5$ to 7 mice per group. *$P < 0.05$. (**F**) Pyruvate tolerance test (PTT) was performed. (**G**) Relative AUC for PTT results (relative to PBS-treated WT mice) is shown. Error bars represent SEM. $n = 3$ to 5 mice per group. *$P < 0.05$.

and *Angptl4*$^{-/-}$ mice, plasma insulin concentrations were increased 15 min after glucose administration but returned to basal values within 30 min (Fig. 1C). In dexamethasone-treated wild-type mice, plasma insulin concentrations were similar at all three time points measured (Fig. 1C). In dexamethasone-treated *Angptl4*$^{-/-}$ mice, plasma insulin concentrations remained high 30 min after glucose administration (Fig. 1C). This sustained increase in plasma insulin in *Angptl4*$^{-/-}$ mice presumably overcame insulin resistance, explaining the normal glucose tolerance of dexamethasone-treated *Angptl4*$^{-/-}$ mice. This finding suggested that, in contrast to wild-type mice, pancreatic islet β cells of *Angptl4*$^{-/-}$ mice could better compensate than those in wild-type mice for the presence of insulin resistance. The lack of difference in insulin concentrations between dexamethasone-treated *Angptl4*$^{-/-}$ or wild-type mice at the 30-min time point in the IPGTT again demonstrated that dexamethasone-treated wild-type mice were more severely glucose-intolerant than *Angptl4*$^{-/-}$ mice.

To further assess whether *Angptl4* depletion could protect mice from glucocorticoid-induced insulin resistance, we performed insulin tolerance tests (ITTs) to monitor and compare the dexamethasone effect on whole-body insulin sensitivity of wild-type and *Angptl4*$^{-/-}$ mice. Dexamethasone treatment significantly worsened insulin tolerance in wild-type mice (Fig. 1, D and E). *Angptl4*$^{-/-}$ mice were less insulin-tolerant than wild-type mice in the absence of dexamethasone treatment (Fig. 1, D and E). However, dexamethasone-treated *Angptl4*$^{-/-}$ mice had similar insulin tolerance to control wild-type mice and less impaired insulin tolerance compared to dexamethasone-treated wild-type mice (Fig. 1, D and E). These results demonstrated that a lack of *Angptl4* prevented the whole-body insulin insensitivity induced by glucocorticoid exposure.

We next performed PTTs to assess the effect of glucocorticoids on hepatic gluconeogenesis. After pyruvate injection, dexamethasone-treated wild-type mice had higher plasma glucose concentrations than control mice over the course of the experiment (Fig. 1, F and G). In contrast, plasma glucose concentrations in PBS- and dexamethasone-treated *Angptl4*$^{-/-}$ mice were similar after pyruvate injection (Fig. 1, F and G). These results demonstrated that the ability of glucocorticoids to stimulate hepatic gluconeogenesis was attenuated in mice lacking *Angptl4*.

To identify the organ that contributes to the insulin sensitivity observed upon *Angptl4* depletion, we monitored the activity of Akt in epididymal WAT (eWAT), liver, and gastrocnemius muscle after 10 min of insulin treatment in control and dexamethasone-treated wild-type and *Angptl4*$^{-/-}$ mice. Akt is phosphorylated at Ser^{473} and Thr^{308} upon insulin treatment (*17*), and we monitored phosphorylation of Thr^{308} as an indicator for Akt activation. Insulin treatment caused an increase in the phosphorylation of Akt in the liver and gastrocnemius muscle of control wild-type mice but not in those of dexamethasone-treated wild-type mice (Fig. 2, A and B). These results demonstrated that dexamethasone treatment prevented insulin activation of Akt in these two tissues. In contrast, insulin treatment increased the phosphorylation

of Akt in the liver and gastrocnemius muscle of *Angptl4*$^{-/-}$ mice, whether they were untreated or given dexamethasone (Fig. 2, A and B). Thus, in the absence of *Angptl4*, insulin still activated Akt in the liver and gastrocnemius muscle even in the presence of dexamethasone. For eWAT, insulin treatment increased the phosphorylation of Akt in both control and dexamethasone-treated wild-type or *Angptl4*$^{-/-}$ mice (Fig. 2C). These results demonstrated that dexamethasone treatment induced insulin resistance in the liver and skeletal muscle of wild-type mice, an effect that was substantially reversed in *Angptl4*$^{-/-}$ mice. In contrast, dexamethasone treatment in eWAT had more complex effects on insulin signaling because insulin-stimulated Akt activation was present both under basal conditions and upon dexamethasone treatment. However, maximal Akt activation was somewhat reduced.

Metabolomic profiling showed alterations of lipid metabolites in the gastrocnemius muscle and liver in control and dexamethasone-treated wild-type and *Angptl4*$^{-/-}$ mice

We hypothesized that Angptl4 was involved in glucocorticoid-induced insulin resistance by mobilizing fatty acids from WAT which were then converted in the liver and skeletal muscle to metabolites that modulated insulin action. To test this model, we performed single reaction monitoring (SRM)–based targeted metabolomic analysis to quantify the concentrations of about 150 common lipid metabolites (data file S1). We focused on the gastrocnemius muscle and liver because they became insulin-resistant upon dexamethasone treatment in our experimental system (Fig. 2, A and B). We found that dexamethasone treatment significantly increased the amounts of 11 metabolites and decreased the amounts of 48 metabolites in the liver of wild-type mice (Fig. 3A and data file S1). Surprisingly, none of the lipid species identified in muscle tissues were significantly increased after dexamethasone treatment in wild-type mice, although nine metabolite species were reduced (data file S1); none of these nine metabolites had previously been associated with the development of insulin resistance.

Six of the 11 metabolites that were increased in wild-type mouse liver by dexamethasone treatment were significantly lower in dexamethasone-treated *Angptl4*$^{-/-}$ mice. These were C18:0 ceramide, C16:0 sphingosine phosphate (S1P), C16:0/C18:1/C16:0 triacylglycerol (TAG), C18:0/C18:1/C18:0 TAG, C18:0/C18:1 diacylglycerol (DAG), and C16:0/C18:1 phosphatidylethanolamine (PE) (Fig. 3B). Although the amounts of ceramides, DAG (*18*, *19*), and S1P (*20*, *21*) have been correlated with the development of insulin resistance, only ceramides have been linked to the glucocorticoid-induced modulation of insulin sensitivity (*11*).

We performed liver histology to visualize the morphological changes of hepatocytes after dexamethasone treatment. For wild-type mice, dexamethasone treatment increased the size of hepatocytes, in which the unstained areas were likely due to the accumulation of triglycerides (fig. S2A). Dexamethasone treatment also increased the size of hepatocytes in *Angptl4*$^{-/-}$ mice (fig. S2A). However, hepatocytes in dexamethasone-treated *Angptl4*$^{-/-}$ mice were smaller than those in dexamethasone-treated wild-type mice (fig. S2A). This finding agrees with reduced induction of triglyceride concentrations in *Angptl4*$^{-/-}$ mouse liver (Fig. 3, A and B). We did not observe statistically significant differences in eWAT weight between control and dexamethasone-treated wild-type and *Angptl4*$^{-/-}$ mice (fig. S2B). This result is likely due to the concomitant stimulation of triglyceride synthesis and lipolysis by dexamethasone in WATs (*13*, *22*).

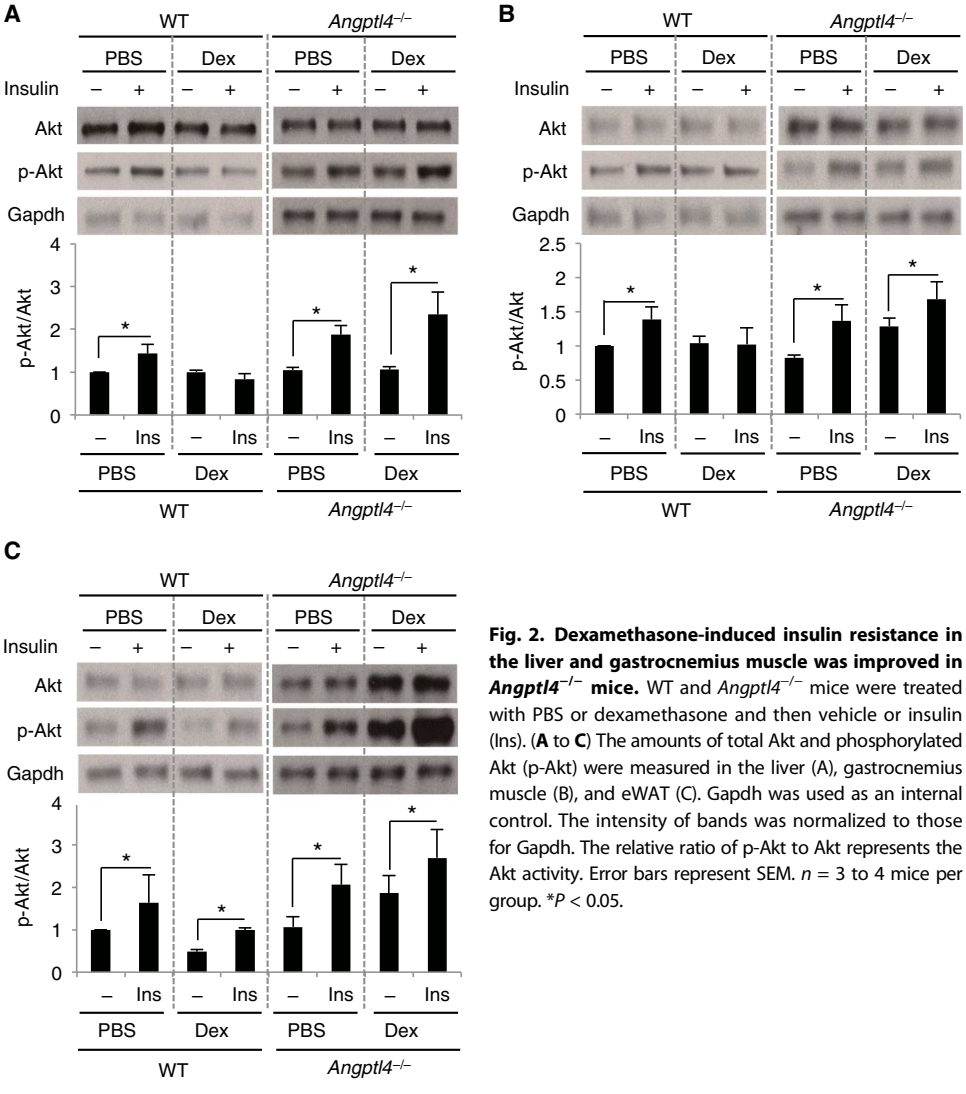

Fig. 2. Dexamethasone-induced insulin resistance in the liver and gastrocnemius muscle was improved in *Angptl4*$^{-/-}$ mice. WT and *Angptl4*$^{-/-}$ mice were treated with PBS or dexamethasone and then vehicle or insulin (Ins). (**A** to **C**) The amounts of total Akt and phosphorylated Akt (p-Akt) were measured in the liver (A), gastrocnemius muscle (B), and eWAT (C). Gapdh was used as an internal control. The intensity of bands was normalized to those for Gapdh. The relative ratio of p-Akt to Akt represents the Akt activity. Error bars represent SEM. $n = 3$ to 4 mice per group. *$P < 0.05$.

Activation of the hepatic ceramide synthetic program was attenuated in *Angptl4*$^{-/-}$ mice

Distinct ceramide species, which are defined by their fatty acyl chain length, can exert specific biological functions (*23*, *24*). Therefore, we expanded our initial SRM-based targeted metabolomic analysis by analyzing multiple ceramide species to determine whether their abundance in the liver was modulated

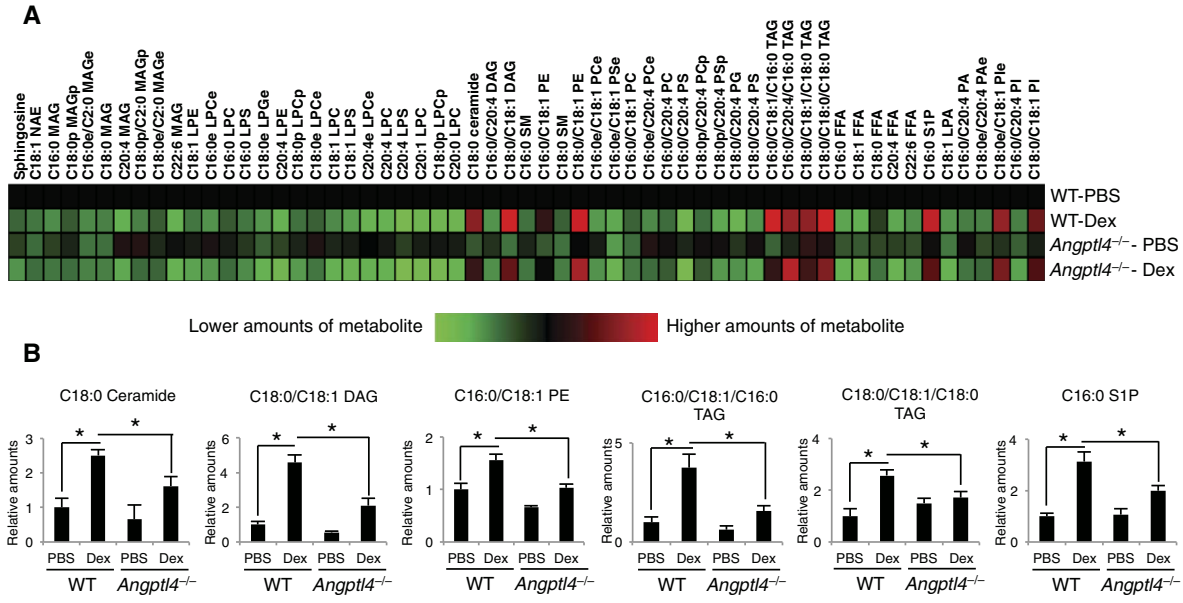

Fig. 3. Metabolomics analysis in the liver and gastrocnemius muscle of control and dexamethasone-treated WT and *Angptl4*$^{-/-}$ mice. WT and *Angptl4*$^{-/-}$ mice were treated with PBS or dexamethasone for 7 days. (**A**) Metabolomics analysis was performed on hepatic lipids. The heat map shows metabolites that are significantly altered in content ($P < 0.05$) upon dexamethasone treatment in the livers of WT mice. The relative content was displayed in the heat map compared to the WT PBS group. Red shading on the heat map indicates higher relative amounts, and green shading represents lower relative amounts. (**B**) Six lipid metabolites that were significantly increased in abundance in dexamethasone-treated WT mice liver but not in dexamethasone-treated *Angptl4*$^{-/-}$ mice are shown. Error bars represent SEM. $n = 4$ mice per group. *$P < 0.05$.

by dexamethasone treatment. Sixteen of the ceramide species were similar in abundance between control wild-type and *Angptl4*$^{-/-}$ mice (Fig. 4A). However, dexamethasone treatment markedly increased the amounts of a subset of ceramide species, including C16:0, C18:0, C20:0, C20:1, C20:2, C22:1, C22:2, C24:2, and C26:0 ceramides in wild-type mouse liver (Fig. 4A). These ceramide species were lower in abundance in the livers of dexamethasone-treated *Angptl4*$^{-/-}$ mice (Fig. 4A). C24:1 ceramides were the only species that were reduced by dexamethasone treatment in the livers of wild-type mice (Fig. 4A), a decrease that was more pronounced in the livers of dexamethasone-treated *Angptl4*$^{-/-}$ mice.

The simplest model to explain the overall reduction of ceramide species in the livers of dexamethasone-treated *Angptl4*$^{-/-}$ mice is that the stimulation of lipolysis by dexamethasone in WAT is diminished in *Angptl4*$^{-/-}$ mice, which then decreases the availability of palmitate for hepatic ceramide synthesis. We found that dexamethasone treatment for 7 days increased plasma palmitate (C16:0 free fatty acid) concentrations by about 50% in wild-type mice (Fig. 4B). In dexamethasone-treated *Angptl4*$^{-/-}$ mice, plasma palmitate concentrations were 27% lower than those of dexamethasone-treated wild-type mice, although this difference was not statistically significant (Fig. 4B). Plasma stearic acid (C18:0 free fatty acid) concentrations were also augmented by dexamethasone treatment in wild-type mice, and this induction was significantly reduced in dexamethasone-treated *Angptl4*$^{-/-}$ mice (Fig. 4B). However, dexamethasone treatment did not affect the concentrations of C18:1, C20:4, and C22:6 free fatty acids in wild-type mice (Fig. 4B). Plasma C16:0, C18:0, and C20:4 free fatty acid concentrations were either significantly or trending higher in control *Angptl4*$^{-/-}$ mice than those in control wild-type mice (Fig. 4B). These results likely reflect the higher activity of LPL in the plasma of *Angptl4*$^{-/-}$ mice (*25*). We also measured the plasma concentrations of representative ceramide species and found that the increase in the amounts of C16:0, C18:0, and C20:4 ceramides in wild-type mice induced by dexamethasone was attenuated in *Angptl4*$^{-/-}$ mice (Fig. 4C).

Although dexamethasone treatment increased fatty acid flux from WAT to the liver, only 11 lipid species were increased by glucocorticoids in the livers of wild-type mice. This observation suggested that, in addition to increasing the availability of hepatic fatty acids, dexamethasone may stimulate specific metabolic pathways that regulate ceramide synthesis. Therefore, we tested this idea by analyzing the expression of genes encoding enzymes involved in ceramide synthesis. In agreement with previous observations, we found that *Spt2*, *Cers3*, *Cers4*, *Cers5*, and *Cers6*, which are genes encoding enzymes in the de novo ceramide synthetic pathway, were all induced by dexamethasone treatment (Fig. 4D and fig. S1) (*11*). The expression of *Smpd1*, which encodes an enzyme that converts sphingomyelins to ceramides (Fig. 4E), was also augmented by dexamethasone (Fig. 4D and fig. S1). Dexamethasone also increased the expression of *Sgms1*, which encodes an enzyme that converts ceramides to sphingomyelins (Fig. 4E). Counterintuitively, the induction of *Sgms1* and *Smpd1* by dexamethasone promotes the bidirectional interconversion of ceramides and sphingomyelins, reminiscent of the effect of glucocorticoid in both promoting hepatic glycogen synthesis and gluconeogenesis (*2*, *26*). Because we observed decreased levels of sphingomyelins (C16:0 and C18:0) upon dexamethasone treatment (Fig. 3A), we postulated that induction of *Smpd1* likely dominates over the *Sgms1* induction by dexamethasone. Finally, the stimulation of *Sphk1* expression, a gene that encodes an enzyme that converts sphingosine to S1P (Fig. 4E), likely explains the decreased sphingosine and increased S1P amounts in the livers of dexamethasone-treated wild-type mice (Fig. 3A).

In *Angptl4*$^{-/-}$ mice, the ability of dexamethasone to augment the expression of *Cers3*, *Cers4*, *Cers5*, *Cers6*, and *Sphk1* was impaired, whereas the induction of *Spt2* and *Smpd1* by dexamethasone was not affected

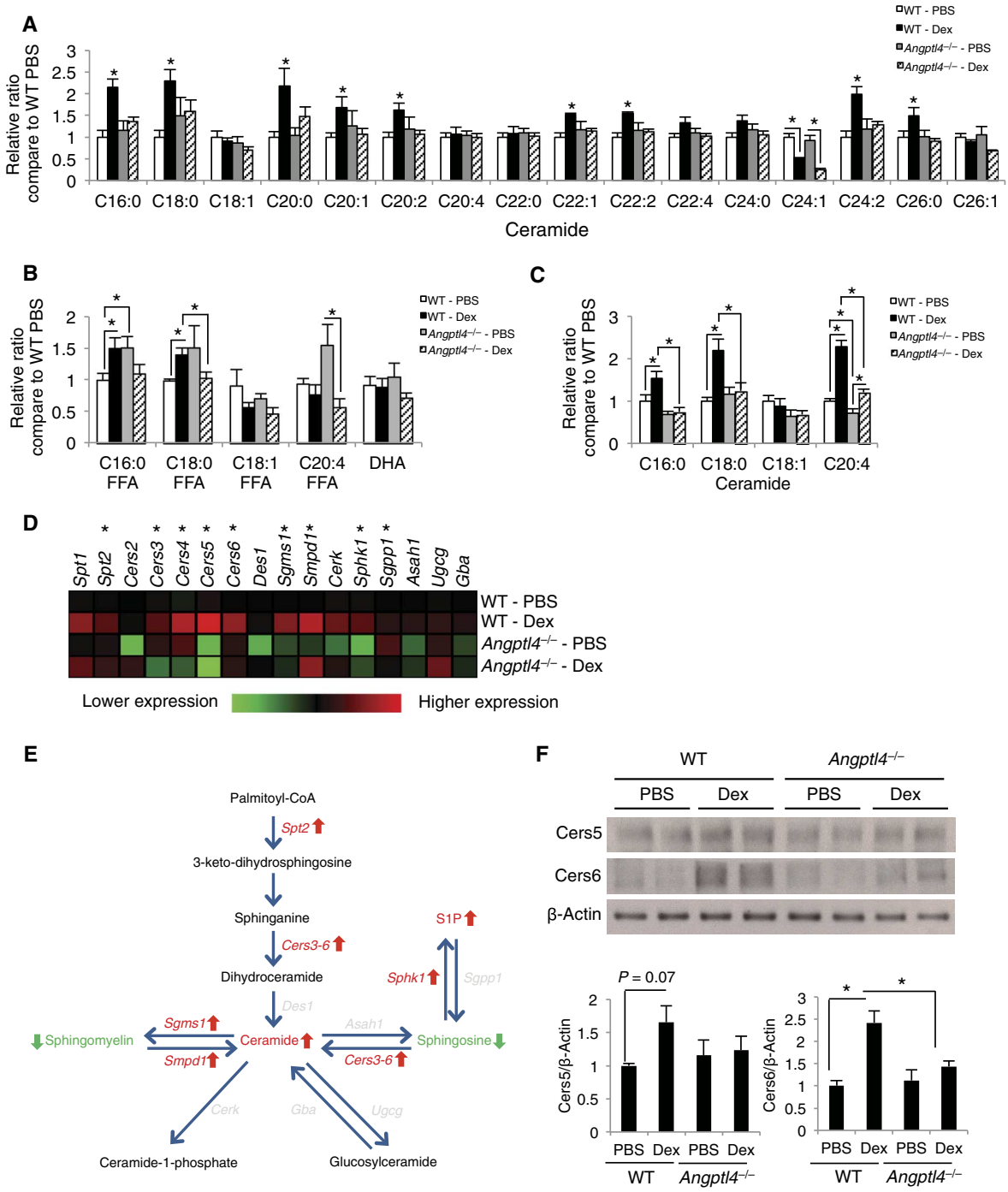

Fig. 4. Dexamethasone-activated hepatic ceramide synthetic program was attenuated in *Angptl4*$^{-/-}$ mice. WT and *Angptl4*$^{-/-}$ mice were treated with PBS or dexamethasone for 7 days. (**A** to **C**) The concentrations of 16 different ceramide species in the liver (A), 5 different free fatty acids (FFAs) in plasma (B), and 4 ceramide species in plasma (C) of these mice were measured. $n = 4$ mice per group. (**D**) The expression of genes encoding enzymes involved in ceramide production was monitored using quantitative polymerase chain reaction (qPCR). The heat map shows the relative expression compared to that in the WT PBS group. Red shading on the heat map indicates higher expression, and green shading represents lower expression. The changes in fold induction are shown in fig. S1. $n = 16$ mice per group. (**E**) Schematic representation of ceramide synthesis pathways. The genes and metabolites that were induced by dexamethasone in WT mice liver are shown in red. The metabolites that were reduced by dexamethasone are shown in green. (**F**) The abundance of Cers5 and Cers6 proteins was monitored using Western blot. The bar graph represents the average intensity of bands normalized to those for Gapdh. Error bars represent SEM. $n = 3$ to 4 mice per group. *$P < 0.05$.

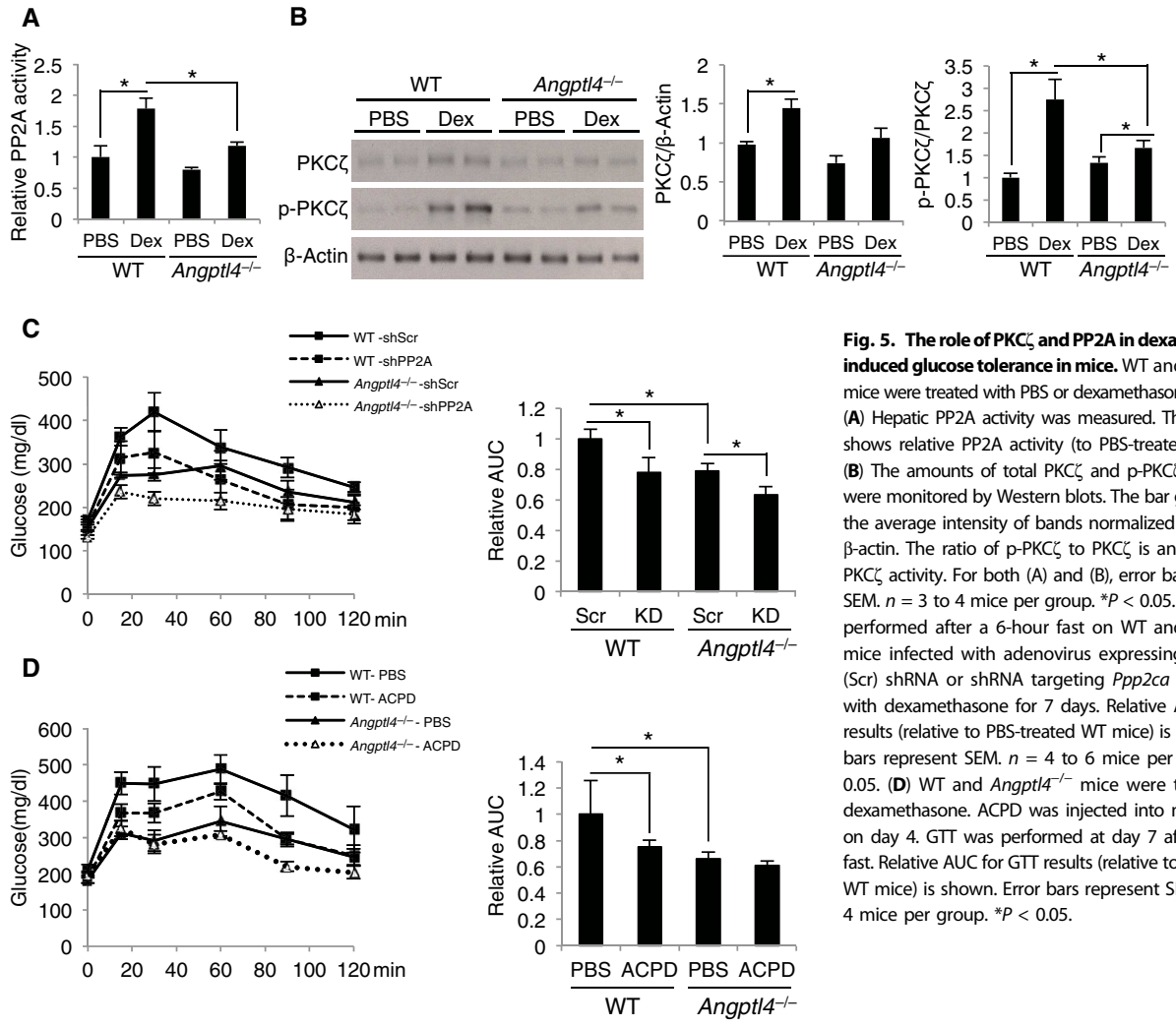

Fig. 5. The role of PKCζ and PP2A in dexamethasone-induced glucose tolerance in mice. WT and *Angptl4*$^{-/-}$ mice were treated with PBS or dexamethasone for 7 days. (**A**) Hepatic PP2A activity was measured. The bar graph shows relative PP2A activity (to PBS-treated WT mice). (**B**) The amounts of total PKCζ and p-PKCζ in the liver were monitored by Western blots. The bar graph shows the average intensity of bands normalized to those for β-actin. The ratio of p-PKCζ to PKCζ is an indicator of PKCζ activity. For both (A) and (B), error bars represent SEM. $n = 3$ to 4 mice per group. *$P < 0.05$. (**C**) GTT was performed after a 6-hour fast on WT and *Angptl4*$^{-/-}$ mice infected with adenovirus expressing scrambled (Scr) shRNA or shRNA targeting *Ppp2ca* and treated with dexamethasone for 7 days. Relative AUC for GTT results (relative to PBS-treated WT mice) is shown. Error bars represent SEM. $n = 4$ to 6 mice per group. *$P < 0.05$. (**D**) WT and *Angptl4*$^{-/-}$ mice were treated with dexamethasone. ACPD was injected into mice starting on day 4. GTT was performed at day 7 after a 6-hour fast. Relative AUC for GTT results (relative to PBS-treated WT mice) is shown. Error bars represent SEM. $n = 3$ to 4 mice per group. *$P < 0.05$.

(Fig. 4D). The decreased expression of *Sphk1* could explain the reduced S1P amounts in the livers of dexamethasone-treated *Angptl4*$^{-/-}$ mice compared to dexamethasone-treated wild-type mice (Fig. 3, A and B). Overall, these results suggested that the reduction in ceramide production in the livers of *Angptl4*$^{-/-}$ mice was due to both diminished substrate availability and impairment in the induction of ceramide synthetic enzymes by dexamethasone (Fig. 4E). To confirm that the gene expression changes were reflected at the protein level, we performed immunoblotting for Cers5 and Cers6 as representative enzymes in ceramide synthesis. The abundance of these two proteins was increased by dexamethasone in the livers of wild-type mice but not in *Angptl4*$^{-/-}$ mice (Fig. 4F). Overall, these gene expression analyses agreed with the metabolomic results, which demonstrated complex effects of dexamethasone on ceramide metabolism (Fig. 4E).

The activation of downstream signaling effectors by ceramides was impaired in dexamethasone-treated *Angptl4*$^{-/-}$ mice

Protein phosphatase 2A (PP2A) and protein kinase Cζ (PKCζ) act downstream of ceramide-initiated signaling (*27*, *28*). To estimate the PP2A activity, we measured dephosphorylation of threonine-phosphopeptides using immunoprecipitates of PP2A from liver lysates. We found that dexamethasone treatment increased PP2A activity in the livers of wild-type mice (≈1.8-fold), an effect that was reduced in those of *Angptl4*$^{-/-}$ mice (Fig. 5A). We found that autophosphorylation of Thr^{560} of PKCζ, which is required for PKCζ activation (*29*), was increased by dexamethasone treatment in the livers of wild-type mice, an effect that was reduced in those of *Angptl4*$^{-/-}$ mice (Fig. 5B). These results validated the concept that dexamethasone treatment stimulates ceramide-initiated signaling in the liver, which is impaired in the absence of *Angptl4*.

To test whether PP2A is involved in glucose intolerance induced by glucocorticoids, wild-type and *Angptl4*$^{-/-}$ mice were infected with adenovirus expressing scrambled small hairpin RNA (shRNA) (control) or shRNA targeting *Ppp2ca*, which encodes a PP2A catalytic subunit. Western blots confirmed a significant reduction in the protein abundance of the PP2A catalytic subunit by *Ppp2ca* shRNA in mouse liver (fig. S3A). Moreover, PP2A activity was about 60% lower in the livers of mice expressing *Ppp2ca* shRNA than that of control mice (fig. S3B). IPGTTs revealed that reducing hepatic PP2A activity improved glucose tolerance in dexamethasone-treated wild-type mice (Fig. 5C). Dexamethasone-treated *Angptl4*$^{-/-}$ mice were more glucose-tolerant than dexamethasone-treated wild-type mice (Fig. 5C). Reducing hepatic *Ppp2ca* expression in dexamethasone-treated *Angptl4*$^{-/-}$ mice further improved glucose tolerance (Fig. 5C).

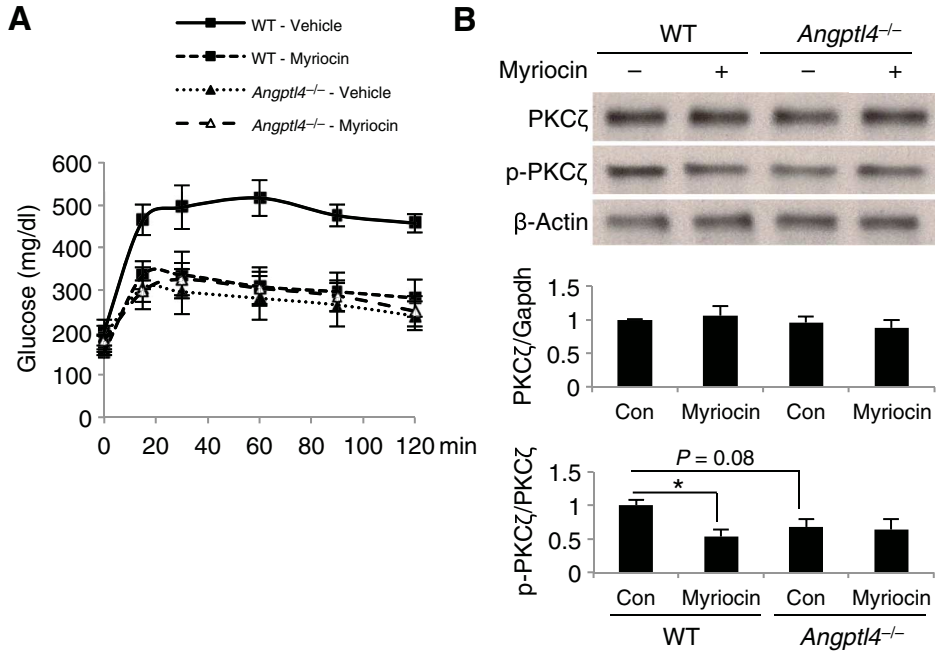

Fig. 6. Myriocin improved glucose tolerance in dexamethasone-treated WT but not in *Angptl4*$^{-/-}$ mice. (**A**) WT and *Angptl4*$^{-/-}$ mice were treated with dexamethasone. Myriocin was injected intraperitoneally into mice starting on day 4. GTT was then performed after 6 hours of fasting. (**B**) Western blots were performed to monitor the amounts of total PKCζ and p-PKCζ in the liver of mice treated with or without myriocin. The bar graph shows the average intensity of bands normalized to those for β-actin. The ratio of p-PKCζ to PKCζ is an indicator of PKCζ activity. Error bars represent SEM. n = 3 to 4 mice per group for (A) and (B). *P < 0.05.

To evaluate the role of PKCζ in glucocorticoid-induced glucose intolerance, wild-type and *Angptl4*$^{-/-}$ mice were injected with or without 2-acetyl-1,3-cyclopentanedione (ACPD), an inhibitor of atypical PKC, PKCζ, and PKCι (*30*, *31*) for the final 4 days of the 7-day dexamethasone course, which reduced PKCζ activity (fig. S3C). IPGTTs showed that ACPD treatment significantly improved glucose tolerance in dexamethasone-treated wild-type but not in *Angptl4*$^{-/-}$ mice (Fig. 5D). Overall, these results suggested that both PP2A and PKCζ are involved in dexamethasone-induced glucose intolerance.

The inhibition of ceramide synthesis by myriocin reduces dexamethasone-induced insulin resistance in wild-type but not in *Angptl4*$^{-/-}$ mice

Inhibiting ceramide synthesis by the Spt1 and Spt2 inhibitor myriocin (*32*) reduces dexamethasone-induced insulin resistance (*11*). If the major role for Angptl4 in dexamethasone-induced insulin resistance is to increase hepatic ceramide production, we hypothesized that blocking ceramide synthesis would improve insulin sensitivity in dexamethasone-treated wild-type but not in dexamethasone-treated *Angptl4*$^{-/-}$ mice. Consistent with our model, we found that treatment with the ceramide synthase inhibitor myriocin attenuated dexamethasone-induced glucose intolerance in wild-type mice but not in *Angptl4*$^{-/-}$ mice (Fig. 6A).

We also monitored the activity of PKCζ to validate our hypothesis that the effect of myriocin was mediated through ceramide generation. We focused on PKCζ because reducing PKCζ activity, similar to myriocin treatment, did not further improved glucose tolerance in dexamethasone-treated *Angptl4*$^{-/-}$ mice (Fig. 5D). Myriocin treatment markedly decreased the phosphorylation of PKCζ in dexamethasone-treated wild-type mice (Fig. 6B). These results suggested that myriocin treatment reduced the ceramide-initiated signaling that was induced by dexamethasone. In contrast, in dexamethasone-treated *Angptl4*$^{-/-}$ mice, myriocin treatment did not affect PKCζ phosphorylation (Fig. 6B). These results agreed with the lack of effect of myriocin on glucose tolerance in dexamethasone-treated *Angptl4*$^{-/-}$ mice (Fig. 6B).

DISCUSSION

The molecular mechanisms underlying the antagonistic effect of glucocorticoids on whole-body insulin sensitivity are not clear. Our present studies demonstrated that *Angptl4*, a primary target gene of glucocorticoid receptor in hepatocytes and adipocytes (*12*), plays a key role in glucocorticoid-induced insulin resistance. We have previously shown that Angptl4 is required for glucocorticoid-induced WAT lipolysis and that purified Angptl4 proteins can directly enhance lipolysis in primary adipocytes (*14*). Here, we showed that Angptl4 was required for glucocorticoid-induced ceramide production and ceramide-initiated signaling in the liver. On the basis of these results, we propose that Angptl4 participates in glucocorticoid-induced insulin resistance by promoting lipolysis in WAT, which mobilizes fatty acids that are taken up by the liver for ceramide production (Fig. 7). In addition to promoting adipocyte lipolysis, Angptl4 also inhibits extracellular LPL (*15*, *16*). Our present studies mainly focused on the lipolytic effect of Angptl4 in glucocorticoid-induced insulin resistance. However, we cannot exclude a role for the inhibitory effect of Angptl4 on LPL in regulating insulin sensitivity. Reducing LPL activity may lead to hypertriglyceridemia, which could also contribute to insulin resistance.

The simplest model for Angptl4 action in glucocorticoid-induced insulin resistance is that enhancing WAT lipolysis provides the precursors, such as palmitate, for hepatic ceramide production. On the basis of our results, Angptl4 action also provided signals needed for glucocorticoids to activate ceramide synthetic pathways in the liver, because without Angptl4, the ability of dexamethasone to stimulate specific ceramide synthetic genes was attenuated (Fig. 7). Glucocorticoid treatment increases the expression of several genes involved in ceramide synthesis in the liver (*11*) through unknown mechanisms. Chromatin immunoprecipitation sequencing analysis in mouse liver has identified glucocorticoid receptor binding sites in or nearby genomic regions of several ceramide synthetic genes, such as *Cers6*, *Cers3*, and *Spt2* (*33*). However, whether these genes are indeed glucocorticoid receptor primary target genes would require further study. In addition to the direct activation of ceramide synthetic genes by glucocorticoid receptor, another potential mechanism is that the fatty acids generated by Angptl4-induced lipolysis in WAT provide the signals to act with glucocorticoids to regulate ceramide synthetic genes. Saturated fatty acids activate nuclear factor κB (NFκB) to stimulate ceramide synthetic

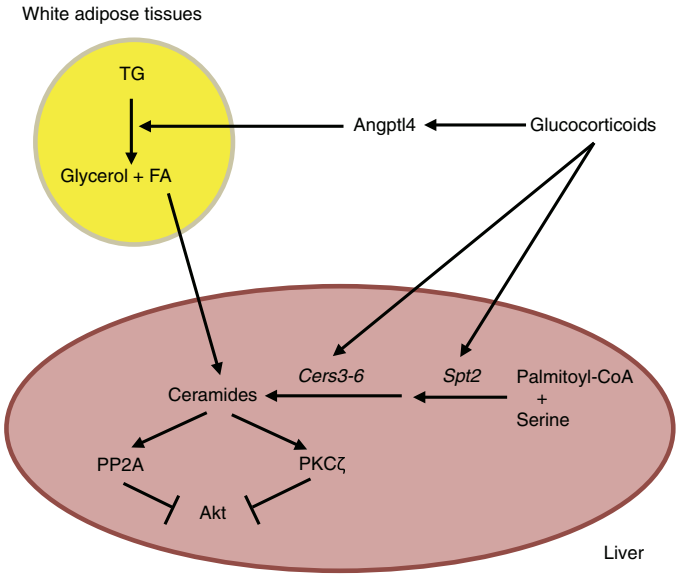

Fig. 7. The proposed model for the role of Angptl4 in glucocorticoid-induced hepatic insulin resistance. Glucocorticoid activates the expression of *Angptl4*, which promotes lipolysis in WAT. Fatty acids (FAs) generated from lipolysis of triglycerides (TGs) serve as both precursors for ceramide synthesis (such as palmitate) and also signals to act with glucocorticoids to increase the expression of *Cers3*, *Cers4*, *Cers5*, and *Cers6*. *Spt1* and *Spt2* expression is also induced by glucocorticoids, though this induction does not require *Angptl4*. Ceramides subsequently activate PKCζ and PP2A, which inhibit Akt and result in insulin resistance.

genes in the liver (*23*, *34*), although the glucocorticoid receptor antagonizes NFκB responses (*35*, *36*). Alternatively, fatty acids can serve as ligands for peroxisome proliferator–activated receptor α and γ (PPARα and PPARγ, respectively) (*37*, *38*). PPARα increases ceramide production in the heart (*39*), skin (*40*), and trophoblasts (*41*), whereas PPARγ promotes ceramide synthesis in keratinocytes (*42*).

It was intriguing that our results showed an increase in various ceramide species by dexamethasone in the liver and that dexamethasone treatment increased the expression of at least four ceramide synthases (*Cers3-6*). Each ceramide synthase is responsible for synthesizing different species of ceramides, and various studies indicate that different ceramide species exert distinct physiological functions (*23*, *24*). For example, the deletion of *Cers6* gene in the liver, which results in decreased C16:0 ceramide concentrations, protects mice from high-fat diet–induced insulin resistance (*43*). In contrast, haploinsufficiency of *Cers2* gene in mice results in the development of insulin resistance (*44*). In the livers of these *Cers2* heterozygous mice, the amounts of C16:0 ceramides and the abundance of Cers5 and Cers6, two proteins that are responsible for the production of C16:0 ceramides, are increased. Furthermore, increasing acid ceramidase expression in the liver decreases the concentrations of C16:0 and C18:0 ceramides that are correlated to the reduction in both PKCζ activity and the development of insulin resistance (*31*). Overall, these results suggest that C16:0 ceramides suppress insulin sensitivity. On the basis of our results, the abundance of Cers5 and Cers6 proteins and C16:0 ceramides in the liver was induced by dexamethasone. Thus, Cers5 and/or Cers6 could potentially act downstream of Angptl4 to confer dexamethasone-induced insulin resistance. Moreover, in addition to ceramides, our metabolomics studies identified dexamethasone-induced increases in other lipid metabolites, including C18:0/18:1 DAG and C16:0 S1P, which are increased in insulin resistance. DAG amounts in the liver are associated with the development of insulin resistance (*18*, *19*), and the amounts of C18:0/18:1 DAG are positively correlated with homeostatic model assessment–insulin resistance (*45*). In contrast, S1P inhibits insulin action through S1P receptor 2 ($S1P_2$) in the liver (*20*, *21*). Note that our results have not identified the specific ceramide species and/or metabolites involved in glucocorticoid-induced insulin resistance. The potential role of Cers3-6 and Sphk1 on glucocorticoid-induced insulin resistance remains to be established.

Although PKCζ and PP2A are downstream of ceramides, their roles in glucocorticoid-induced insulin resistance have not been examined. Here, we showed that both were involved in glucose intolerance induced by dexamethasone treatment. Reducing PP2A abundance but not PKCζ activity further improved glucose tolerance in dexamethasone-treated $Angptl4^{-/-}$ mice, suggesting that the stimulation of PKCζ in the liver by glucocorticoids mainly required Angptl4, whereas there are other glucocorticoid-regulated mechanisms that can activate PP2A. It is unclear whether PP2A and PKCζ act in the same or the parallel pathway to modulate insulin actions.

The increase in ceramide concentrations in the liver explains the role of Angptl4 in glucocorticoid-induced hepatic insulin resistance. However, insulin response in the gastrocnemius muscle was also improved in $Angptl4^{-/-}$ mice. It is surprising that in the gastrocnemius muscle, only nine metabolites were affected by dexamethasone treatment, and none of them have been previously linked to insulin sensitivity. It is possible that the metabolites modulated by dexamethasone treatment to induce insulin resistance in the gastrocnemius muscle were not in the list of target metabolomics experiments we conducted. Notably, ceramides are mainly associated with very-low-density lipoprotein (VLDL) in plasma (*46*), and plasma ceramide concentrations have been negatively associated with insulin sensitivity (*47*, *48*). Therefore, it is also possible that ceramides produced in the liver are mobilized to the gastrocnemius muscle to inhibit insulin action (*49*). This model is somewhat supported by our observation that plasma ceramide concentrations were augmented by dexamethasone in wild-type but not in $Angptl4^{-/-}$ mice (Fig. 4C).

High-fat diet feeding causes inflammation in WAT. Secretion of interleukin-6 from macrophages in WAT increases, which promotes WAT lipolysis and in turn induces hepatic insulin resistance (*50*). Although the induction of WAT lipolysis is also involved in the glucocorticoid-induced development of insulin resistance, glucocorticoid exposure actually suppresses, rather than promotes, inflammation in WAT (*51*). Thus, the glucocorticoid-induced increase in *Angptl4* expression, rather than cytokine production, may be the key step in glucocorticoid-induced insulin resistance. However, Angptl4 is unlikely to be the only mediator of the suppressive effect of glucocorticoids on insulin action, and a network of glucocorticoid primary target genes are likely needed to exert the effect of glucocorticoids on whole-body insulin sensitivity. Regardless, our studies suggest that Angptl4 plays a critical role in triggering interorgan communication between the WAT and the liver, leading to the suppression of insulin action. Overall, these results fill an important gap in our understanding of the metabolic functions of glucocorticoid. Furthermore, targeting Angptl4 may be a promising strategy to dissociate the beneficial anti-inflammatory effects of glucocorticoids from adverse effects such as insulin resistance.

METHODS

Animals

$Angptl4^{-/-}$ mice were provided by the laboratories of A. Nagy (Samuel Lunenfeld Research Institute, Mount Sinai Hospital) and

J. Gordon (Washington University) (*52*). *Angptl4*$^{-/-}$ mice were generated on a mixed B6:129 Sv background. *Angptl4*$^{+/+}$ mice (wild-type mice) were the littermates of *Angptl4*$^{-/-}$ mice. Male (7 to 12 weeks old) mice were used in this study. The genotyping method was performed as previously described (*52*). To test insulin signaling, we injected the mice with insulin (1 U per body weight) for 10 min, and Western blot analysis was performed on various tissues. The Office of Laboratory Animal Care at the University of California, Berkeley, approved all the animal experiments (AUP-2014-08-6617).

Drug administration

Male (7 to 12 weeks old) *Angptl4*$^{+/+}$ (wild-type) and *Angptl4*$^{-/-}$ mice were treated with dexamethasone (~0.42 mg/kg) for 7 days through drinking water. Water-soluble dexamethasone (Sigma, D2915) was dissolved in PBS (25 mg/ml). Notably, water-soluble dexamethasone contains 65 mg of dexamethasone per gram of powder. We prepared drinking water that contains 0.0025 g of dexamethasone per liter and based on our estimate that a 30-g mouse drinks about 3.5 to 5 ml of water per day. In myriocin experiments, myriocin (0.5 mg/kg body weight) was dissolved in PBS and was injected intraperitoneally to mice on the last 4 days of dexamethasone treatment. For ACPD (Sigma, A155) treatment, mice were injected subcutaneously with ACPD (10 mg/kg) dissolved in PBS for 4 days.

IPGTT, ITT, and PTT

Mice were fasted for 6 or 16 hours for GTT and PTT. Mice were injected with glucose (1 g/kg body weight), insulin (1 U/kg body weight, Sigma, I0516-5ML), or sodium pyruvate (1 mg/kg body weight, Spectrum Chemical, SO193) intraperitoneally. Blood samples (one drop from tail vein) were obtained at the 0-, 30-, 60-, 90-, and 120-min time points to measure glucose levels using CONTOUR Blood Glucose Monitoring System (Contour, Bayer). Blood was also collected during different time points of GTT for measuring plasma insulin concentrations.

Lipidomic profiling

Liver tissues and gastrocnemius muscle tissues were used for lipidomic profiling. Lipid metabolites were extracted in 4 ml of a 2:1:1 mixture of chloroform/methanol/Tris buffer with inclusion of internal standards C12:0 dodecylglycerol (10 nmol) and pentadecanoic acid (10 nmol). Organic and aqueous layers were separated by centrifugation at 1000*g* for 5 min, and the organic layer was collected, dried down under N_2, and dissolved in 120 μl of chloroform, of which 10 μl was analyzed by both SRM-based liquid chromatography–tandem mass spectrometry (LC-MS/MS) or untargeted LC-MS. LC separation was achieved with a Luna reverse-phase C5 column (50 mm × 4.6 mm with 5-μm-diameter particles, Phenomenex). Mobile phase A was composed of a 95:5 ratio of water/methanol, and mobile phase B consisted of a 60:35:5 ratio of 2-propanol/methanol/and water. Solvent modifiers (0.1% formic acid with 5 mM ammonium formate and 0.1% ammonium hydroxide) were used to assist ion formation and to improve the LC resolution in both positive and negative ionization modes, respectively. The flow rate for each run started at 0.1 ml/min for 5 min to alleviate backpressure associated with injecting chloroform. The gradient started at 0% B and increased linearly to 100% B over the course of 45 min with a flow rate of 0.4 ml/min, followed by an isocratic gradient of 100% B for 17 min at 0.5 ml/min before equilibrating for 8 min at 0% B with a flow rate of 0.5 ml/min.

MS analysis was performed with an electrospray ionization source on an Agilent 6430 QQQ LC-MS/MS. The capillary voltage was set to 3.0 kV, and the fragmentor voltage was set to 100 V. The drying gas temperature was 350°C, the drying gas flow rate was 10 liters/min, and the nebulizer pressure was 35 psi. Representative metabolites were quantified by SRM of the transition from precursor to product ions at associated collision energies. Data were normalized to the internal standards and also external standard curves of metabolite classes against the internal standards, and concentrations were calculated as relative metabolite concentrations compared to controls. These internal standards were added alongside dodecylglycerol and pentadecanoic acid in the 2:1:1 chloroform/methanol/Tris buffer mixture.

Western blot

The protein concentrations of samples were measured using bicinchoninic acid (BCA) protein assay (Thermo Scientific, 23228). Proteins (~30 μg) were mixed with 1X NuPAGE LDS Sample Buffer (ThermoFisher, NP0007) and 1X NuPAGE Sample Reducing Agent (ThermoFisher, NP0009), boiled for 5 min before applying to SDS–polyacrylamide gel electrophoresis. The following are the antibodies we used in this study: anti-Gapdh (Santa Cruz, sc-25778), anti-Akt (Cell Signaling, 9272s), anti–phospho-Akt (Cell Signaling, 9275s), anti-Cers5 (Life Technologies, PA-520570), anti-Cers6 (Santa Cruz, sc-100554), anti–β-actin (Santa Cruz, sc-47778), anti-PKCζ (Santa Cruz, sc-216), anti–phospho-PKCζ (T410, Cell Signaling, 2060S), anti-Ppp2ca (Cell Signaling, 2041S). The intensity of the bands was quantified using ImageJ software (National Institutes of Health) and normalized to Gapdh or β-actin.

PP2A activity assay

The PP2A activity in the liver lysate was detected using PP2A Immunoprecipitation Phosphatase Assay kit (Millipore, 17-313FR) following the manufacturer's protocol.

Real-time qPCR

Total RNA was isolated from liver tissues using TRIzol reagent (Invitrogen, 15596018). Reverse transcription was performed as follows: 0.5 μg of total RNA, 4 μl of 2.5 mM dNTP, and 2 μl of 15 μM random primers (New England Biolabs, S1254S) were mixed at a volume of 16 μl and incubated at 70°C for 5 min. A 4-μl cocktail containing 25 U of Moloney Murine Leukemia Virus (M-MuLV) Reverse Transcriptase (New England Biolabs, M0253S), 10 U of RNasin Plus (Promega, N261B), and 2 μl of 10x M-MuLV Reverse Transcriptase Reaction Buffer (New England Biolabs, B0253S) were added, and samples were incubated at 42°C for 1 hour and then at 95°C for 5 min. The cDNA was diluted and used for real-time qPCR using the Power Eva qPCR SuperMix Kit (Biochain, K5057400) following the manufacturer's protocol. qPCR was performed on the StepOne PCR System (Applied Biosystems) and analyzed with the $\Delta\Delta C_t$ method, as supplied by the manufacturer (Applied Biosystems). *Rpl19* gene expression was used for internal normalization. Primer sequences used in this study are listed in table S1.

Adenovirus

Adenovirus expressing scramble shRNA or shRNA targeting *Ppp2ca* was purchased from Vector Biolabs. The targeting sequences for *Ppp2ca* are CGACGAGTGTTTAAGGAAATA, which has been previously reported (*53*). Mice were injected by tail vein with 1×10^9 plaque-forming units (pfu) adenovirus/mouse.

Histology

Livers from treated mice were harvested and fixed in 10% neutral buffered formalin (Sigma, HT501128). Liver was embedded, sectioned, and stained for hematoxylin and eosin by the University of California, San Francisco (UCSF) Liver Center Pathology and Imaging Core (San Francisco, CA). Images were taken at the UC Berkeley Biological Imaging Facility (Berkeley, CA) using the Zeiss AxioImager M1 at ×20 magnification. Each image shows a portion of the hepatic lobule. One image from each treatment group was shown. At least two animals were analyzed for each treatment group. Multiple sections were performed for each liver.

Statistics

Data are expressed as SEM for each group, and comparisons were analyzed by Student's *t* test.

SUPPLEMENTARY MATERIALS

www.sciencesignaling.org/cgi/content/full/10/489/eaai7905/DC1

Fig. S1. Expression analysis of genes involved in ceramide metabolism.

Fig. S2. Liver histology and WAT weight in dexamethasone-treated wild-type and *Angptl4*$^{-/-}$ mice.

Fig. S3. PP2A abundance and PKCζ activity in mice infected with adenovirus expressing *Ppp2ca* shRNA or treated with a PKCζ inhibitor.

Table S1. qPCR primer list.

Data file S1. Lipidomic data in the liver and gastrocnemius muscle of control or dexamethasone-treated wild-type and *Angptl4*$^{-/-}$ mice.

REFERENCES AND NOTES

1. R. C. Andrews, B. R. Walker, Glucocorticoids and insulin resistance: Old hormones, new targets. *Clin. Sci. (Lond.)* **96**, 513–523 (1999).
2. T. Kuo, A. McQueen, T.-C. Chen, J.-C. Wang, Regulation of glucose homeostasis by glucocorticoids. *Adv. Exp. Med. Biol.* **872**, 99–126 (2015).
3. G. Di Dalmazi, U. Pagotto, R. Pasquali, V. Vicennati, Glucocorticoids and type 2 diabetes: From physiology to pathology. *J. Nutr. Metab.* **2012**, 525093 (2012).
4. K. Ohshima, N. S. Shargill, T. M. Chan, G. A. Bray, Effects of dexamethasone on glucose transport by skeletal muscles of obese (ob/ob) mice. *Int. J. Obes.* **13**, 155–163 (1989).
5. L. L. Gathercole, I. J. Bujalska, P. M. Stewart, J. W. Tomlinson, Glucocorticoid modulation of insulin signaling in human subcutaneous adipose tissue. *J. Clin. Endocrinol. Metab.* **92**, 4332–4339 (2007).
6. J. Buren, H. X. Liu, J. Jensen, J. W. Eriksson, Dexamethasone impairs insulin signalling and glucose transport by depletion of insulin receptor substrate-1, phosphatidylinositol 3-kinase and protein kinase B in primary cultured rat adipocytes. *Eur. J. Endocrinol.* **146**, 419–429 (2002).
7. J. Ruzzin, A. S. Wagman, J. Jensen, Glucocorticoid-induced insulin resistance in skeletal muscles: Defects in insulin signalling and the effects of a selective glycogen synthase kinase-3 inhibitor. *Diabetologia* **48**, 2119–2130 (2005).
8. T. C. Brennan-Speranza, H. Henneicke, S. J. Gasparini, K. I. Blankenstein, U. Heinevetter, V. C. Cogger, D. Svistounov, Y. Zhang, G. J. Cooney, F. Buttgereit, C. R. Dunstan, C. Gundberg, H. Zhou, M. J. Seibel, Osteoblasts mediate the adverse effects of glucocorticoids on fuel metabolism. *J. Clin. Invest.* **122**, 4172–4189 (2012).
9. A. Ekstrand, C. Saloranta, J. Ahonen, C. Grönhagen-Riska, L. C. Groop, Reversal of steroid-induced insulin resistance by a nicotinic-acid derivative in man. *Metabolism* **41**, 692–697 (1992).
10. N. Venkatesan, M. B. Davidson, A. Hutchinson, Possible role for the glucose-fatty acid cycle in dexamethasone-induced insulin antagonism in rats. *Metabolism* **36**, 883–891 (1987).
11. W. L. Holland, J. T. Brozinick, L.-P. Wang, E. D. Hawkins, K. M. Sargent, Y. Liu, K. Narra, K. L. Hoehn, T. A. Knotts, A. Siesky, D. H. Nelson, S. K. Karathanasis, G. K. Fontenot, M. J. Birnbaum, S. A. Summers, Inhibition of ceramide synthesis ameliorates glucocorticoid-, saturated-fat-, and obesity-induced insulin resistance. *Cell Metab.* **5**, 167–179 (2007).
12. S. K. Koliwad, T. Kuo, L. E. Shipp, N. E. Gray, F. Backhed, A. Y.-L. So, R. V. Farese Jr., J.-C. Wang, Angiopoietin-like 4 (ANGPTL4, fasting-induced adipose factor) is a direct glucocorticoid receptor target and participates in glucocorticoid-regulated triglyceride metabolism. *J. Biol. Chem.* **284**, 25593–25601 (2009).
13. C.-Y. Yu, O. Mayba, J. V. Lee, J. Tran, C. Harris, T. P. Speed, J.-C. Wang, Genome-wide analysis of glucocorticoid receptor binding regions in adipocytes reveal gene network involved in triglyceride homeostasis. *PLOS ONE* **5**, e15188 (2010).
14. N. E. Gray, L. N. Lam, K. Yang, A. Y. Zhou, S. Koliwad, J.-C. Wang, Angiopoietin-like 4 (Angptl4) protein is a physiological mediator of intracellular lipolysis in murine adipocytes. *J. Biol. Chem.* **287**, 8444–8456 (2012).
15. K. Yoshida, T. Shimizugawa, M. Ono, H. Furukawa, Angiopoietin-like protein 4 is a potent hyperlipidemia-inducing factor in mice and inhibitor of lipoprotein lipase. *J. Lipid Res.* **43**, 1770–1772 (2002).
16. W. Dijk, S. Kersten, Regulation of lipoprotein lipase by Angptl4. *Trends Endocrinol. Metab.* **25**, 146–155 (2014).
17. D. R. Alessi, M. Andjelkovic, B. Caudwell, P. Cron, N. Morrice, P. Cohen, B. A. Hemmings, Mechanism of activation of protein kinase B by insulin and IGF-1. *EMBO J.* **15**, 6541–6551 (1996).
18. F. R. Jornayvaz, G. I. Shulman, Diacylglycerol activation of protein kinase Cε and hepatic insulin resistance. *Cell Metab.* **15**, 574–584 (2012).
19. V. T. Samuel, K. F. Petersen, G. I. Shulman, Lipid-induced insulin resistance: Unravelling the mechanism. *Lancet* **375**, 2267–2277 (2010).
20. S. Fayyaz, J. Henkel, L. Japtok, S. Krämer, G. Damm, D. Seehofer, G. P. Püschel, B. Kleuser, Involvement of sphingosine 1-phosphate in palmitate-induced insulin resistance of hepatocytes via the $S1P_2$ receptor subtype. *Diabetologia* **57**, 373–382 (2014).
21. S. Fayyaz, L. Japtok, B. Kleuser, Divergent role of sphingosine 1-phosphate on insulin resistance. *Cell Physiol. Biochem.* **34**, 134–147 (2014).
22. C. Harris, D. J. Roohk, M. Fitch, B. M. Boudignon, B. P. Halloran, M. K. Hellerstein, Large increases in adipose triacylglycerol flux in Cushingoid CRH-Tg mice are explained by futile cycling. *Am. J. Physiol. Endocrinol. Metab.* **304**, E282–E293 (2013).
23. B. Chaurasia, S. A. Summers, Ceramides – Lipotoxic inducers of metabolic disorders. *Trends Endocrinol. Metab.* **26**, 538–550 (2015).
24. J.-W. Park, W.-J. Park, A. H. Futerman, Ceramide synthases as potential targets for therapeutic intervention in human diseases. *Biochim. Biophys. Acta* **1841**, 671–681 (2014).
25. A. Köster, Y. B. Chao, M. Mosior, A. Ford, P. A. Gonzalez-DeWhitt, J. E. Hale, D. Li, Y. Qiu, C. C. Fraser, D. D. Yang, J. G. Heuer, S. R. Jaskunas, P. Eacho, Transgenic angiopoietin-like (angptl)4 overexpression and targeted disruption of angptl4 and angptl3: Regulation of triglyceride metabolism. *Endocrinology* **146**, 4943–4950 (2005).
26. R. N. Margolis, R. T. Curnow, The role of insulin and glucocorticoids in the regulation of hepatic glycogen metabolism: Effect of fasting, refeeding, and adrenalectomy. *Endocrinology* **113**, 2113–2119 (1983).
27. R. T. Dobrowsky, C. Kamibayashi, M. C. Mumby, Y. A. Hannun, Ceramide activates heterotrimeric protein phosphatase 2A. *J. Biol. Chem.* **268**, 15523–15530 (1993).
28. G. Muller, M. Ayoub, P. Storz, J. Rennecke, D. Fabbro, K. Pfizenmaier, PKC zeta is a molecular switch in signal transduction of TNF-alpha, bifunctionally regulated by ceramide and arachidonic acid. *EMBO J.* **14**, 1961–1969 (1995).
29. Y. Kanoh, G. Bandyopadhyay, M. P. Sajan, M. L. Standaert, R. V. Farese, Thiazolidinedione treatment enhances insulin effects on protein kinase C-ζ/λ activation and glucose transport in adipocytes of nondiabetic and Goto-Kakizaki type II diabetic rats. *J. Biol. Chem.* **275**, 16690–16696 (2000).
30. M. P. Sajan, R. A. Ivey, M. C. Lee, R. V. Farese, Hepatic insulin resistance in ob/ob mice involves increases in ceramide, aPKC activity, and selective impairment of Akt-dependent FoxO1 phosphorylation. *J. Lipid Res.* **56**, 70–80 (2015).
31. J. Y. Xia, W. L. Holland, C. M. Kusminski, K. Sun, A. X. Sharma, M. J. Pearson, A. J. Sifuentes, J. G. McDonald, R. Gordillo, P. E. Scherer, Targeted induction of ceramide degradation leads to improved systemic metabolism and reduced hepatic steatosis. *Cell Metab.* **22**, 266–278 (2015).
32. Y. Miyake, Y. Kozutsumi, S. Nakamura, T. Fujita, T. Kawasaki, Serine palmitoyltransferase is the primary target of a sphingosine-like immunosuppressant, ISP-1/myriocin. *Biochem. Biophys. Res. Commun.* **211**, 396–403 (1995).
33. L. Grøntved, S. John, S. Baek, Y. Liu, J. R. Buckley, C. Vinson, G. Aguilera, G. L. Hager, C/EBP maintains chromatin accessibility in liver and facilitates glucocorticoid receptor recruitment to steroid response elements. *EMBO J.* **32**, 1568–1583 (2013).
34. W. L. Holland, B. T. Bikman, L.-P. Wang, G. Yuguang, K. M. Sargent, S. Bulchand, T. A. Knotts, G. Shui, D. J. Clegg, M. R. Wenk, M. J. Pagliassotti, P. E. Scherer, S. A. Summers, Lipid-induced insulin resistance mediated by the proinflammatory receptor TLR4 requires saturated fatty acid-induced ceramide biosynthesis in mice. *J. Clin. Invest.* **121**, 1858–1870 (2011).
35. N. A. S. Rao, M. T. McCalman, P. Moulos, K.-J. Francoijs, A. Chatziioannou, F. N. Kolisis, M. N. Alexis, D. J. Mitsiou, H. G. Stunnenberg, Coactivation of GR and NFKB alters the repertoire of their binding sites and target genes. *Genome Res.* **21**, 1404–1416 (2011).
36. K. De Bosscher, W. Vanden Berghe, G. Haegeman, The interplay between the glucocorticoid receptor and nuclear factor-κB or activator protein-1: Molecular mechanisms for gene repression. *Endocr. Rev.* **24**, 488–522 (2003).
37. A. Georgiadi, S. Kersten, Mechanisms of gene regulation by fatty acids. *Adv. Nutr.* **3**, 127–134 (2012).

38. L. la Cour Poulsen, M. Siersbaek, S. Mandrup, PPARs: Fatty acid sensors controlling metabolism. *Semin. Cell Dev. Biol.* **23**, 631–639 (2012).
39. M. Baranowski, A. Błachnio, P. Zabielski, J. Górski, PPARα agonist induces the accumulation of ceramide in the heart of rats fed high-fat diet. *J. Physiol. Pharmacol.* **58**, 57–72 (2007).
40. M. Rivier, I. Castiel, I. Safonova, G. Ailhaud, S. Michel, Peroxisome proliferator-activated receptor-α enhances lipid metabolism in a skin equivalent model. *J. Invest. Dermatol.* **114**, 681–687 (2000).
41. I. L. M. H. Aye, X. Gao, S. T. Weintraub, T. Jansson, T. L. Powell, Adiponectin inhibits insulin function in primary trophoblasts by PPARα-mediated ceramide synthesis. *Mol. Endocrinol.* **28**, 512–524 (2014).
42. M. Baranowski, A. Blachnio, P. Zabielski, J. Gorski, Pioglitazone induces de novo ceramide synthesis in the rat heart. *Prostaglandins Other Lipid Mediat.* **83**, 99–111 (2007).
43. S. M. Turpin, H. T. Nicholls, D. M. Willmes, A. Mourier, S. Brodesser, C. M. Wunderlich, J. Mauer, E. Xu, P. Hammerschmidt, H. S. Brönneke, A. Trifunovic, G. LoSasso, F. T. Wunderlich, J.-W. Kornfeld, M. Blüher, M. Kronke, J. C. Brüning, Obesity-induced CerS6-dependent $C_{16:0}$ ceramide production promotes weight gain and glucose intolerance. *Cell Metab.* **20**, 678–686 (2014).
44. S. Raichur, S. T. Wang, P. W. Chan, Y. Li, J. Ching, B. Chaurasia, S. Dogra, M. K. Öhman, K. Takeda, S. Sugii, Y. Pewzner-Jung, A. H. Futerman, S. A. Summers, CerS2 haploinsufficiency inhibits β-oxidation and confers susceptibility to diet-induced steatohepatitis and insulin resistance. *Cell Metab.* **20**, 687–695 (2014).
45. T. Galbo, R. J. Perry, M. J. Jurczak, J.-P. Camporez, T. C. Alves, M. Kahn, B. A. Guigni, J. Serr, D. Zhang, S. Bhanot, V. T. Samuel, G. I. Shulman, Saturated and unsaturated fat induce hepatic insulin resistance independently of TLR-4 signaling and ceramide synthesis in vivo. *Proc. Natl. Acad. Sci. U.S.A.* **110**, 12780–12785 (2013).
46. A. H. Merrill Jr., S. Lingrell, E. Wang, M. Nikolova-Karakashian, T. R. Vales, D. E. Vance, Sphingolipid biosynthesis de novo by rat hepatocytes in culture. Ceramide and sphingomyelin are associated with, but not required for, very low density lipoprotein secretion. *J. Biol. Chem.* **270**, 13834–13841 (1995).
47. J. M. Haus, S. R. Kashyap, T. Kasumov, R. Zhang, K. R. Kelly, R. A. Defronzo, J. P. Kirwan, Plasma ceramides are elevated in obese subjects with type 2 diabetes and correlate with the severity of insulin resistance. *Diabetes* **58**, 337–343 (2009).
48. X. Lopez, A. B. Goldfine, W. L. Holland, R. Gordillo, P. E. Scherer, Plasma ceramides are elevated in female children and adolescents with type 2 diabetes. *J. Pediatr. Endocrinol. Metab.* **26**, 995–998 (2013).
49. J. P. Kirwan, Plasma ceramides target skeletal muscle in type 2 diabetes. *Diabetes* **62**, 352–354 (2013).
50. R. J. Perry, J.-P. Camporez, R. Kursawe, P. M. Titchenell, D. Zhang, C. J. Perry, M. J. Jurczak, A. Abudukadier, M. S. Han, X.-M. Zhang, H.-B. Ruan, X. Yang, S. Caprio, S. M. Kaech, H. S. Sul, M. J. Birnbaum, R. J. Davis, G. W. Cline, K. F. Petersen, G. I. Shulman, Hepatic acetyl CoA links adipose tissue inflammation to hepatic insulin resistance and type 2 diabetes. *Cell* **160**, 745–758 (2015).
51. D. Patsouris, J. G. Neels, W. Fan, P.-P. Li, M. T. Nguyen, J. M. Olefsky, Glucocorticoids and thiazolidinediones interfere with adipocyte-mediated macrophage chemotaxis and recruitment. *J. Biol. Chem.* **284**, 31223–31235 (2009).
52. F. Bäckhed, H. Ding, T. Wang, L. V. Hooper, G. Y. Koh, A. Nagy, C. F. Semenkovich, J. I. Gordon, The gut microbiota as an environmental factor that regulates fat storage. *Proc. Natl. Acad. Sci. U.S.A.* **101**, 15718–15723 (2004).
53. L. Xie, C. Liu, L. Wang, H. P. Gunawardena, Y. Yu, R. Du, D. J. Taxman, P. Dai, Z. Yan, J. Yu, S. P. Holly, L. V. Parise, Y. Y. Wan, J. P. Ting, X. Chen, Protein phosphatase 2A catalytic subunit α plays a MyD88-dependent, central role in the gene-specific regulation of endotoxin tolerance. *Cell Rep.* **3**, 678–688 (2013).

Acknowledgments: We thank H. S. Sul (UC Berkeley) and R. O'Brien (Vanderbilt) for helpful comments on the manuscript. We thank A. Nagy (Samuel Lunenfeld Research Institute, Mount Sinai Hospital) and J. Gordon (Washington University) for providing mice. **Funding:** This work was supported by the NIH (R01DK083591). J.-C.W. is a member of the UCSF Liver Center (P30DK026743). T.-C.C. is supported by the Dr. and Mrs. James C.Y. Soong Fellowship from the University of California. T.K. is supported by the Dissertation Award Fellowship from the University of California Tobacco-Related Diseases Research Program. **Author contributions:** T.-C.C., D.I.B., T.K., D.K.N., and J.-C.W. carried out the conceptualization and methodology for this work. T.-C.C., D.I.B., T.K., R.A.L., M.-L.L., D.J.M., and D.E.C. performed the investigations. T.-C.C., D.I.B., D.K.N., R.A.L., and J.-C.W. wrote the manuscript. Funding was acquired by J.-C.W., and supervision was performed by D.K.N. and J.-C.W. **Competing interests:** The authors declare that they have no competing interests.

Submitted 14 August 2016
Accepted 10 July 2017
Published 25 July 2017
10.1126/scisignal.aai7905

Citation: T.-C. Chen, D. I. Benjamin, T. Kuo, R. A. Lee, M.-L. Li, D. J. Mar, D. E. Costello, D. K. Nomura, J.-C. Wang, The glucocorticoid-Angptl4-ceramide axis induces insulin resistance through PP2A and PKCζ. *Sci. Signal.* **10**, eaai7905 (2017).

The glucocorticoid-Angptl4-ceramide axis induces insulin resistance through PP2A and PKCζ

Tzu-Chieh Chen, Daniel I. Benjamin, Taiyi Kuo, Rebecca A. Lee, Mei-Lan Li, Darryl J. Mar, Damian E. Costello, Daniel K. Nomura and Jen-Chywan Wang

Sci. Signal. **10** (489), eaai7905.
DOI: 10.1126/scisignal.aai7905

Using glucocorticoids without insulin resistance

Inflammation can be reduced with chronic glucocorticoid treatment, which unfortunately is associated with the development of insulin resistance. Glucocorticoids induce the production of the secreted protein Angptl4 and of ceramides, a family of lipid mediators. Chen *et al*. showed that Angptl4 was necessary to induce the expression of genes encoding factors involved in ceramide synthesis in the livers of glucocorticoid-treated mice. Furthermore, Angptl4 was required to stimulate the activity of two downstream effectors of ceramides: PP2A and PKCζ. These results suggest that inhibiting this pathway may alleviate the insulin resistance that occurs with chronic glucocorticoid treatment.

Science Signaling
AAAS

www.sciencesignaling.org/cgi/content/full/10/489/eaai7905/DC1

Supplementary Materials for

The glucocorticoid-Angptl4-ceramide axis induces insulin resistance through PP2A and PKCζ

Tzu-Chieh Chen, Daniel I. Benjamin, Taiyi Kuo, Rebecca A. Lee, Mei-Lan Li, Darryl J. Mar, Damian E. Costello, Daniel K. Nomura, Jen-Chywan Wang*

*Corresponding author. Email: walwang@berkeley.edu

Published 25 July 2017, *Sci. Signal.* **10**, eaai7905 (2017)
DOI: 10.1126/scisignal.aai7905

The PDF file includes:

Other Supplementary Material for this manuscript includes the following:
(available at www.sciencesignaling.org/cgi/content/full/10/489/eaai7905/DC1)

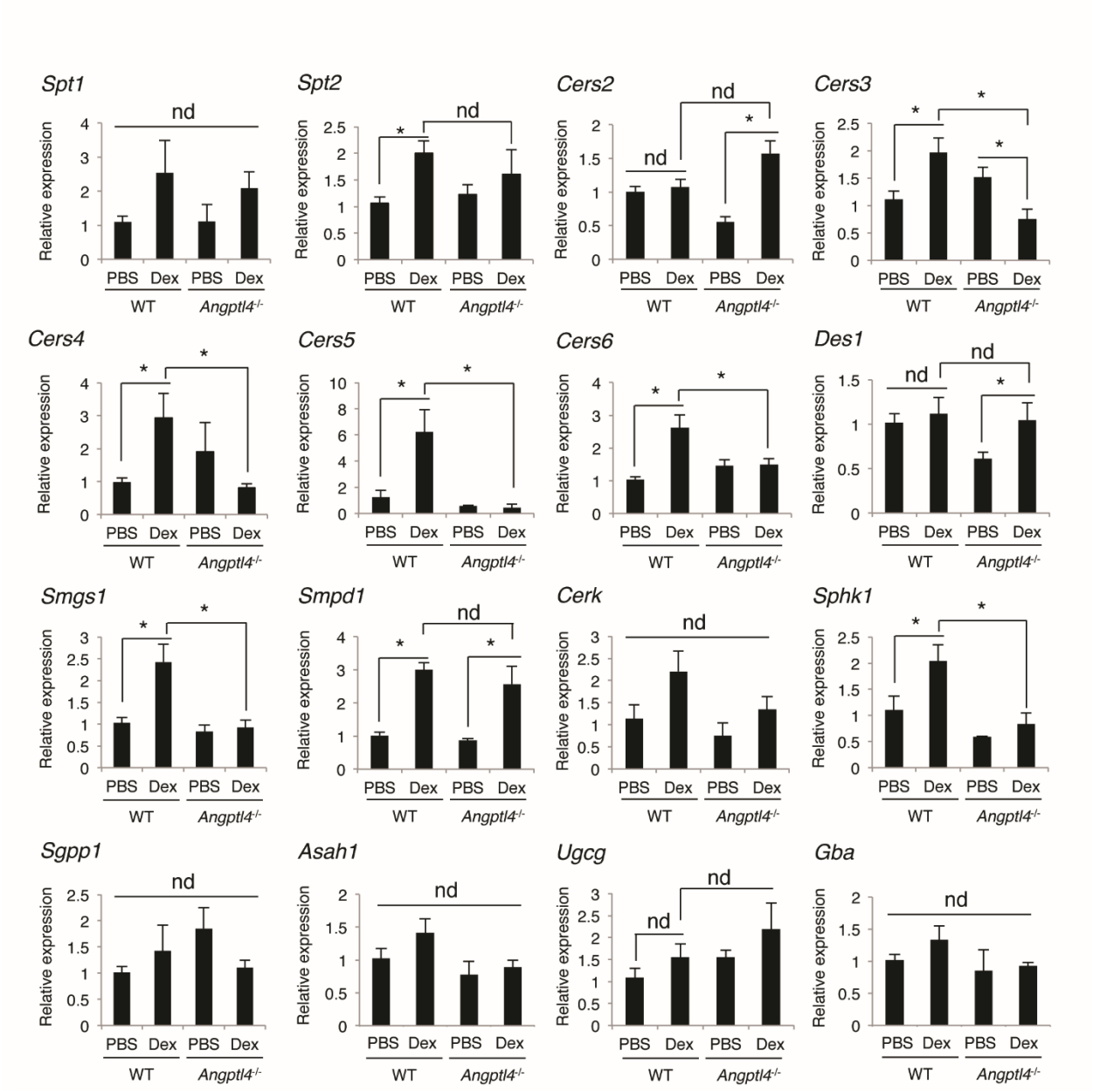

Fig. S1. Expression analysis of genes involved in ceramide metabolism.

WT and *Angptl4*$^{-/-}$ mice were treated with PBS or 0.42 mg/kg of dexamethasone (Dex) for 7 days. Hepatic gene expression patterns were determined by RT-qPCR. Error bars represent S.E.M., n=16 mice per group, and *$p < 0.05$.

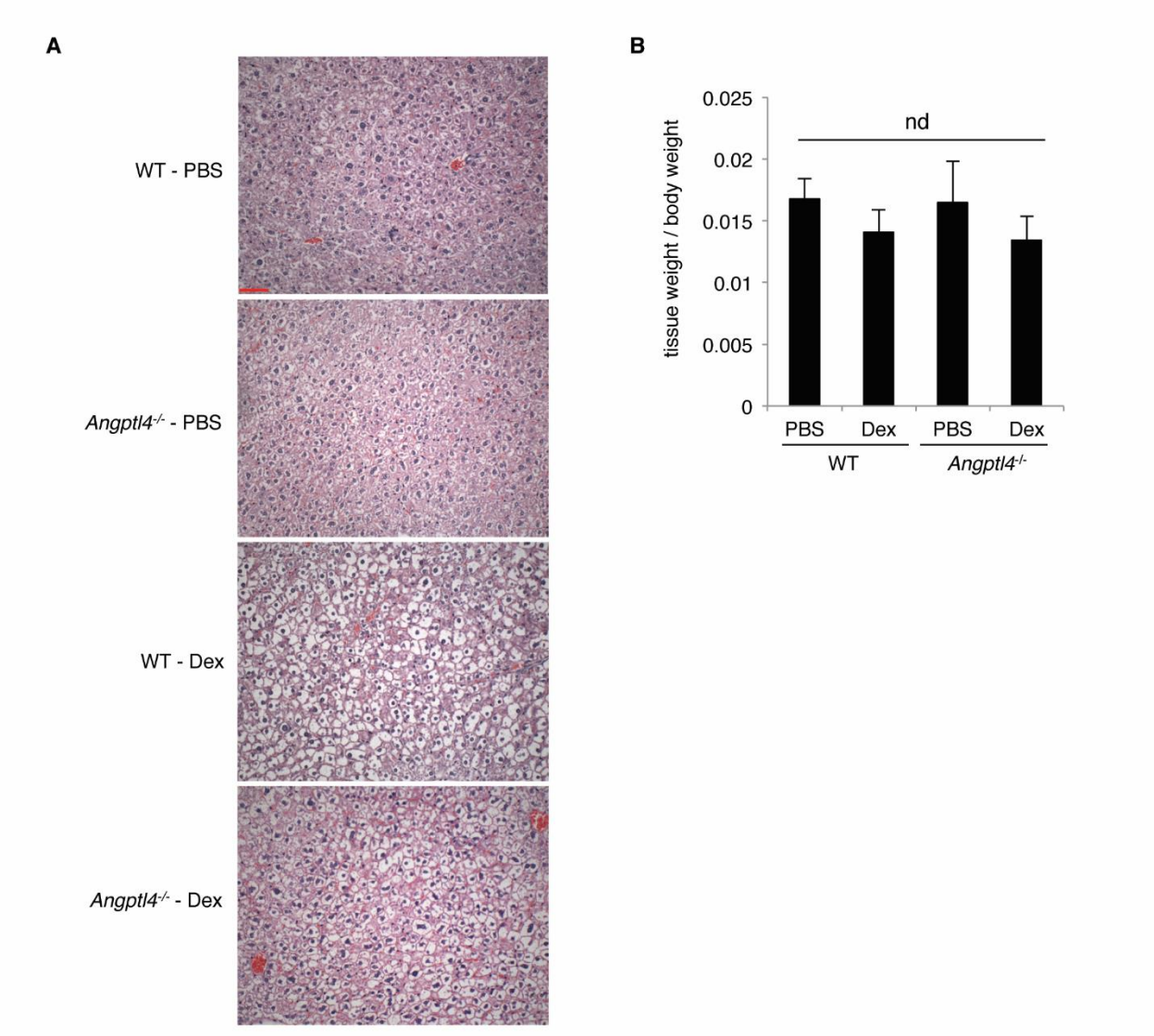

Fig. S2. Liver histology and WAT weight in dexamethasone-treated wild-type and *Angptl4*$^{-/-}$ mice.

WT and *Angptl4*$^{-/-}$ mice were treated with PBS or 0.42 mg/kg of dexamethasone for 7 days prior to the collection of liver and eWAT. (**A**) Livers were fixed in 10% neutral buffered formalin and histology was performed by the UCSF Liver Center Pathology and Imaging Core (San Francisco, CA). For each mouse liver, multiple sections were prepared. Two animals per treatment group were processed for histological analysis. Representative images for each treatment group are

shown. Scale bar (red, bottom left of top panel) represents 60 microns. (**B**) The graph shows the ratio of eWAT weight to total body weight. N=5-6 mice per group.

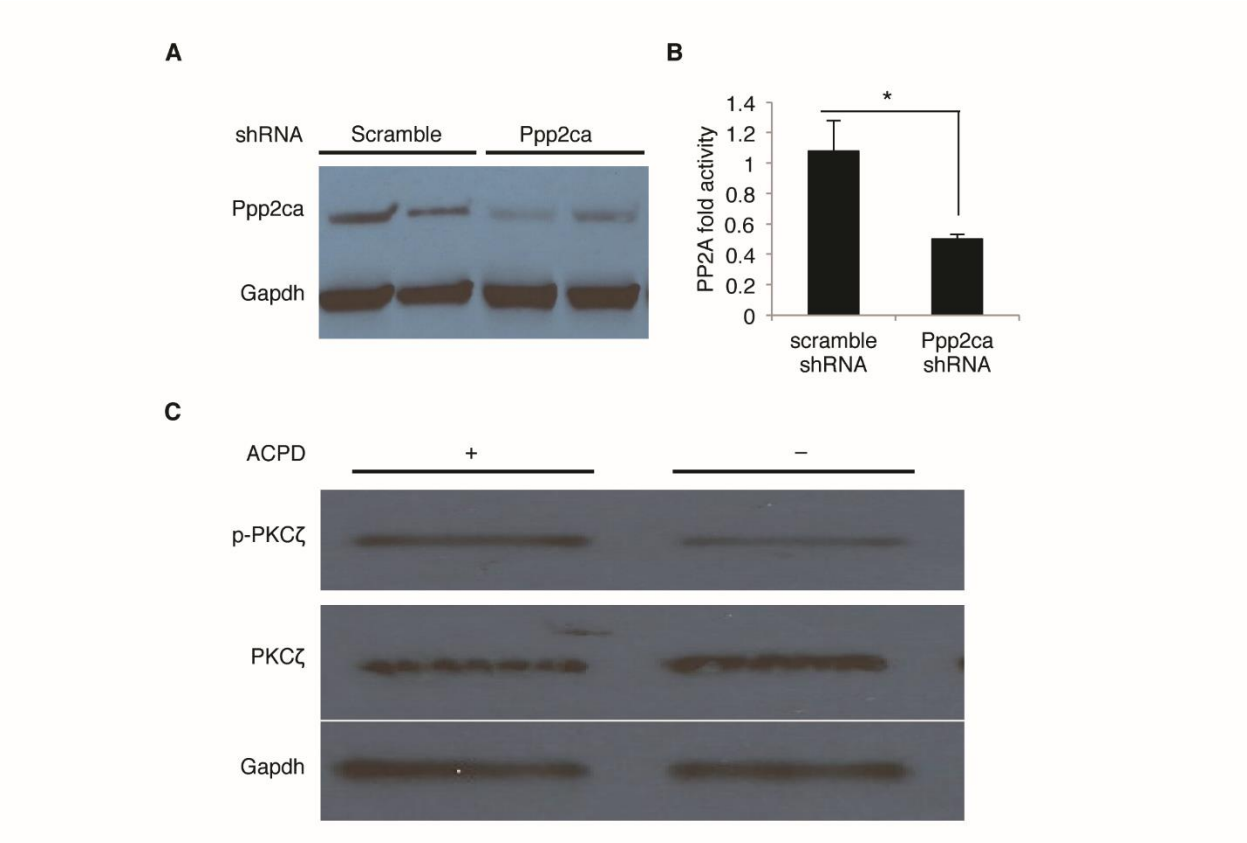

Fig. S3. PP2A abundance and PKCζ activity in mice infected with adenovirus expressing *Ppp2ca* shRNA or treated with a PKCζ inhibitor.

Wild-type mice were infected with $1x10^9$ pfu/mouse of adenovirus expressing scramble shRNA or shRNA targeting *Ppp2ca*. Mice were treated with 0.42 mg/kg of dexamethasone for 7 days. Western blotting was performed to monitor Ppp2ca protein abundance (**A**) and PP2A activity was measured (**B**) in liver. (**C**) Wild-type mice were treated with 0.42 mg/kg of dexamethasone for 7 days. 10 mg/kg of ACPD was injected into mice subcutaneously daily starting from day 4 for 4 days. Western blotting was performed to monitor the amount of p-PKCζ, PKCζ and Gapdh (loading control) in liver.

Table S1. qPCR primer list.

Gene	Forward	Reverse
Spt1	TACTCAGAGACCTCCAGCTG	CACCAGGGATATGCTGTCATC
Spt2	GGAGATGCTGAAGCGGAAC	GTATGAGCTGCTGACAGGCA
Cers2	GGCGCTAGAAGTGGGAAAC	TCGAATGACGAGAAAGAGCA
Cers3	GCTACACCTCTAGCAAATGCAC	ATCTTTCAACCTGGCGCTCT
Cers4	TGTCGTTGACGTTGAGTGAG	AGCAGGCTTCACAGAATTTC
Cers5	ACACTAGCCAATCAGGGCG	GCTGCACTCTCAGGCTCC
Cers6	ACAAAGCAAGATGGCAGGGA	TCCGTGTTCTTCAGGTCTGC
Des1	CACCGGTACCTCGGAGCGGA	GTTTGGGATTGATGAACAGGGGT
Sgms1	CTCATGAGGCCCAACAAGAT	CACCTTCTTGGGTGACCAGT
Smpd1	GGCGAGTACAGCAAGTGTGA	AAGCCATTGACAGGAGTGCT
Cerk	CGGTACTGGTGTCGGAGATCA	GTGAATGCGAACGGATTTTCC
Sphk1	TCCTGGAGGAGGCAGAGATA	CATTAGCCCATTCACCACCT
Sgpp1	TACCCATTGGTGGACCTGAT	CAGGGTATAAGCAGCGTGT
Asah1	ATCAAAAGCTGCCTGGTATGAT	TCCACCCAAGAAATATTCCAA
Ugcg	GGAATGGCCTTGTTCGGCT	CGGCTGTTTGTCTGTTGCC
Gba	ATCTGCTTGGCTCACGAGTT	TGTCGATGAAAGGGGTCTTC